Ocean Sci. Discuss., 11, 2831–2878, 2014
www.ocean-sci-discuss.net/11/2831/2014/
doi:10.5194/osd-11-2831-2014

Ocean Science
Discussions
Open Access

Global representation of tropical cyclone-induced ocean thermal changes using Argo data – Part 1: Methods and results

L. Cheng[1], J. Zhu[1], and R. L. Sriver[2]

[1]International Center for Climate and Environment Sciences, Institute of Atmospheric Physics, Chinese Academy of Sciences, Beijing, China
[2]Department of Atmospheric Sciences, University of Illinois, Urbana-Champaign, IL, USA

Received: 30 October 2014 – Accepted: 14 November 2014 – Published: 9 December 2014

Correspondence to: J. Zhu (jzhu@mail.iap.ac.cn)

Published by Copernicus Publications on behalf of the European Geosciences Union.

Abstract

Argo floats are used to examine tropical cyclone (TC)-induced ocean thermal changes on the global scale by comparing temperature profiles before and after TC passage. We present a footprint method that analyzes cross-track thermal responses along all storm tracks during the period 2004–2012. We combine the results into composite representations of the vertical structure of the average thermal response for two different categories: tropical storms/depressions (TS/TD) and hurricanes. The two footprint composites are functions of three variables: cross-track distance, water depth and time relative to TC passage. We find that this footprint strategy captures the major features of the upper-ocean thermal response to TCs on time scales up to 20 days when compared against previous case study results using in situ measurements. Further, TC effects are distinguishable from background sampling variability, but the significance of this result depends on differences in regional oceanic conditions and the intensity of the TC events. On the global scale, results indicate that hurricanes induce strong upwelling near the storm center, along with downwelling away from the storm, during the first 3 days after storm passage. We also find significant subsurface warming between 30 and 200 m depth for both hurricanes and TS/TDs. On average, the subsurface ocean response persists along storm tracks for up to 20 days down to 200 (400) m depth for TS/TD (Hurricanes), exhibiting peak warming of 0.4 °C at 60 m for hurricanes and 0.2 °C at 35 m for TS/TD. The footprint method shows a weak cooling response between 200 and 400 m, which is significant for Hurricanes but not for TS/TD.

1 Introduction

Tropical cyclones (TCs) provide an effective mechanism to transport heat, mass and nutrients in the ocean, while also exchanging enthalpy with the atmosphere. Multiple lines of evidence from previous observational and modeling studies indicate that these relatively small scale and transient events can influence large scale dynamical pro-

OSD
11, 2831–2878, 2014

cesses in both the ocean (Emanuel, 2001; Sriver and Huber, 2007) and atmosphere (Camargo and Sobel, 2005; Hart, 2011; Jansen et al., 2010; Sriver, 2010).

TCs affect ocean processes and properties on multiple spatial and temporal scales. On scales relevant for climate dynamics, the cumulative effects of TCs on the ocean have been shown to be important for controlling tropical and subtropical ocean temperature patterns through enhanced subsurface mixing (Fedorov et al., 2010; Sriver et al., 2010). It has been hypothesized that increases in this mixing associated with more TC activity is capable of sustaining climates with permanent El Nino-like temperature patterns such as during the early Pliocene, ~ 5 million years ago (Fedorov et al., 2010). On inter-seasonal scales, TC-induced changes in ocean temperature can impact the atmospheric circulations through dynamical connections affecting mid-latitude weather in subsequent winters (Hart, 2011; Hart et al., 2007b). This mechanism, and in general the relatively strong thermal inertia of the ocean, implies a longer memory of tropical cyclones in the ocean than in the atmosphere. On synoptic scales, TC-induced cooling at the surface via enhanced mixing can limit TC intensification (Ginis, 2002).

Understanding the ocean's response to TCs on various spatial and temporal scales is an ongoing area of active research. Since the 1950s, ocean vessels, moorings, and aircraft have been observing ocean conditions in TC-affected regions, which has assisted in building the basic framework for understanding how the ocean responds to TC forcing (Black and Dickey, 2008; Price, 1981, 1983; Price et al., 1994; Shay and Elsberry, 1987; Shay et al., 1989). The response of the upper ocean to TC forcing is typically characterized by surface cooling in the storm wake and subsurface warming caused by a variety of oceanic and atmospheric processes, including generation of near-inertial internal oscillations, geostrophic advection, Ekman pumping, and surface fluxes. Previous studies analyzing the ocean response to TCs have generally been limited by the availability of observations and/or focus on a limited number of storms, resulting in storm-to-storm variations (Bell et al., 2012; Cione and Uhlhorn, 2003; Lin et al., 2009a, b). Until recently, these limitations in data coverage have prevented a global-scale perspective of how TCs affect the ocean.

OSD
11, 2831–2878, 2014

A key difficulty in quantifying the global distribution of TC-induced oceanic thermal response is the lack of all-weather observations with sufficient horizontal, vertical and temporal coverage and resolution. Since the year 2000, Argo profiling floats have provided a global network of in situ ocean surface and subsurface observations. The profiles measure water temperature and salinity from the surface (~ 5 m) to ~ 2000 m depth, even under extreme weather conditions such as TCs. Since 2004, the Argo system has maintained a global array network with resolution of about 3 by 3° in space similar to the XBT-based system (Freeland, 2009). However, the main advantage of the Argo system over previous observational systems is that the floats are more evenly distributed in space and time over the ocean and can observe conditions from greater depths.

Several recent studies have used Argo data to examine ocean conditions under TCs (Lin et al., 2009b; Liu et al., 2007; Mei et al., 2013; Park et al., 2011). Liu et al. (2007) concentrated on northwestern Pacific typhoons, suggesting that TC signals (e.g. sea surface cooling) can be captured by Argo data and these signals are statistically significant. Lin et al. (2009) examined ocean responses under a specific TC (Nargis), showing a clear ocean thermal change from a series of Argo data near the storm. These results support the reliability of Argo observations in severe weather conditions. More recent work examining TC-induced ocean heat content changes in the western Pacific (Park et al., 2011) represents the first attempt to investigate systematically the TC-induced ocean thermal changes on a basin-scale using Argo data. While the authors do identify a TC signature in the Argo data, the TC-induced subsurface temperature response is sensitive to the season in which TCs occur. Furthermore, the TC-induced effect is difficult to separate from the background variability, particularly for weak storms.

Here we propose a new method to examine global TC-ocean interactions using Argo data, which examines all storms globally and characterizes the global mean of the cross-track ocean response to TCs using a footprint method that follows along the storm tracks. We categorize the TC events into two separate groups: Tropical storms/depressions (TS/TD) and Hurricanes. In addition, we separate the ocean's response into two stages: the forced stage (0–3 days relative to storm passage) and the recovery stage (4–20 days relative to storm passage). We use this technique to analyze TC-induced ocean thermal responses on a global scale, accounting for regional variability in background ocean conditions. The paper is organized as follows. We describe the data and footprint methodology in Sect. 2. We examine background variability in Argo data in Sect. 3. We present the results and discussion in Sect. 4. We discuss the caveats of the method in Sect. 5, and Sect. 6 outlines the main conclusions.

2 Data and methods

2.1 Data

Argo floats drift freely at a fixed pressure (usually 1000 m depth and occasionally at 1200 and 1500 m) for about 9–10 days. After this period, the floats descend rapidly to a profiling pressure (usually 2000 m deep) and then rise, collecting near-instantaneous profiles of pressure, temperature, and salinity data on their way to the surface (within a span of about 2 h). The floats remain at the surface for less than one day, transmitting the data collected via a satellite link back to a ground station and allowing the satellite to determine their surface positions. The floats then sink again to their parking depth of ∼ 1000 m and repeat the cycle.

Argo data are available on the website of National Oceanographic Data Center/Global Argo Data Repository. In this study, we use Argo data from January 2004 to December 2012 (downloaded on October 2012). We discard all the profiles in the so-called grey list (Willis et al., 2009). Both delayed mode (data available several months after passing careful quality control processes) and real-time mode (data available to users within two days timeframe) data are used where available, and Argo quality control flags are used to eliminate spurious measurements. We apply an additional "Boundary Check" as follows. If a temperature anomaly within 200–1000 m from a pair (The method of construction of Agro pair is shown in the Sect. 2b) is larger than 2 °C

OSD
11, 2831–2878, 2014

(or smaller than −2 °C), the anomaly is labeled as "spurious". If there are more than 5 "spurious" labels from a single pair, the pair is rejected and all of the "spurious" anomalies are removed. This is a widely used quality control process and helps to get rid of the spikes and anomalous profiles.

Tropical cyclone information comes from the NOAA's Tropical Prediction Center "best track" dataset (http://weather.unisys.com/). The data set contains 6 hourly records of maximum wind speeds, pressure and location. We collect all TC tracks globally between January 2004 to December 2012, totaling 885 events.

2.2 Composite footprint method

We introduce a footprint method that averages all of the TC-induced cross-track (i.e. perpendicular to the storm's direction of motion) ocean temperature changes. Argo pairs are selected to compare temperature profiles before and after storm passage according to the following criteria:

1. The pre-storm Argo profile is within −12 to −2 days before storm passage and the post-storm Argo profile is within 0 to 20 days after storm passage. The 20 day limit is selected because SST changes are largely restored to pre-storm condition within 20 days after storm passage. Furthermore, it is increasingly difficult to separate TC effects from the seasonal cycle of SST on timescales longer than 20 days. Data within −2 to 0 days prior to storm passage are not used as pre-storm reference profiles, since they may be affected by TC processes (e.g. increased heat fluxes ahead of storms).

2. The locations of the pre-storm and post-storm Argo profiles are within 0.2° of each other. Ideally, this comparison should be made at the same location, but it is not possible due to the heterogeneity of the observing system (both in space and time). Therefore, 0.2° is selected as the maximum horizontal distance between the reference and TC-affected Argo floats, since we believe it can both minimize the influences of the background signals (such as meso-scale eddies,

OSD
11, 2831–2878, 2014

boundary currents, and waves) and maximize the size of our TC-affected pairs dataset. By using 0.2°, we implicitly assume that the background ocean variability (not due directly to TC effects) within 0.2° can be neglected when averaging over a large dataset. Sensitivity analyses indicate that background noise and errors contaminate the TC signal when relaxing the Argo pair criterion from 0.2 to 0.5°. Furthermore, horizontal velocities within western boundary ocean currents (e.g. Gulf Stream) and geostrophic vortices within TC regions are typically on the order of O(10–100) $\mathrm{cm\,s^{-1}}$ (Shay et al., 1998). These currents can effectively transport a float more than 0.2° away from its original position on the timescales of our TC analysis. Thus, the maximum 0.2° spatial constraint largely filters these floats from our results, so that we do not contaminate the TC analysis with transient effects of larger-scale dynamics.

3. All of the Argo pairs are within ±8° relative to the center of the storm track, perpendicular to the storm's direction of translation. Thus 16° is assumed to be the maximum cross-track scale of the area affected by TCs. This constraint is a first-order assumption, and we will analyze the horizontal scale of the globally-averaged TC response extensively in the results section.

We define TC-induced ocean thermal changes calculated from Argo pairs using the functional form

$$\mathrm{d}T_{a1} = \mathrm{d}T_{a1}(\mathrm{ID}, \mathrm{dist}, \mathrm{track}, \mathrm{depth}, \delta t)$$

where ID identifies the particular storm, dist is the distance between the observation location and the track center perpendicular to the storm's direction of motion (the cross-track distance in the storm coordinate system), track denotes the spatial location of an Argo pair related to a TC-track (the along-track distance in the storm coordinate system), depth denotes the vertical depth of the temperature anomalies, and δt is the time difference between the observing time of the TC-affected Argo profile and the time of the nearest track center. We define the positive values of dist to be consistent with

OSD
11, 2831–2878, 2014

the asymmetric inertial response (to the right in the Northern Hemisphere and to the left in the Southern Hemisphere), referred to as TC-Track coordinates (Price et al., 2008).

To create a composite representation of the average ocean response, we reduce the 5-dimensional function dT_{a1} to a 3-demesional function by averaging the anomalies along the tracks and over all TCs. We define a track-averaged footprint of ocean thermal changes over all tracks, and we separate the events into two distinct categories: TS/TD and Hurricanes. Track locations with maximum wind speeds less than 63 knots are categorized asTS/TD, and all others are categorized as Hurricanes (this hurricane category represents conditions when a TC is in hurricane status). The footprint is represented as:

$$F_{\mathrm{TSTD}}(\mathrm{dist},\mathrm{depth},\delta t) = \sum_{\mathrm{ID}=1}^{\mathrm{ID}=n_{\mathrm{TSTD}}} \left[\frac{1}{L_{\text{track-TSTD}}(\mathrm{ID})} \int_{\mathrm{track(ID)}} \mathrm{d}T_{a_1}(\mathrm{ID},\mathrm{dist},\mathrm{track},\mathrm{depth},\delta t) d_{\mathrm{track}} \right] \Big/ n_{\mathrm{TSTD}}$$

$$F_{\mathrm{Hur}}(\mathrm{dist},\mathrm{depth},\delta t) = \sum_{\mathrm{ID}=1}^{\mathrm{ID}=n_{\mathrm{Hur}}} \left[\frac{1}{L_{\text{track-Hur}}(\mathrm{ID})} \int_{\mathrm{track(ID)}} \mathrm{d}T_{a_1}(\mathrm{ID},\mathrm{dist},\mathrm{track},\mathrm{depth},\delta t) d_{\mathrm{track}} \right] \Big/ n_{\mathrm{Hur}}$$

In these equations, the temperature anomalies dT_{a1} are averaged along each storm track (denoted as track (ID) for each specific storm) and over all storms (denoted as ID). The length of each storm track is denoted as $L_{\text{track-TSTD}}(\mathrm{ID})$ and $L_{\text{track-Hur}}(\mathrm{ID})$ for an individual TS/TD and hurricane respectively, and the number of storms is denoted as n_{TSTD} and n_{Hur}.

We construct the 3-dimensional footprints by grouping temperature anomalies from TS/TD and Hurricanes respectively with dimensions: dist containing 0.5° bins from −8 to +8° across the track, time containing 0.5 day bins from 0 to 20 days, and depth containing 10 m bins from 5 to 1000 m and 50 m bins from 1000 to 2000 m. In each grid-box, averages of the temperature anomalies are calculated by using temperature anomalies from this box and 14 other adjacent bin-boxes (in time and dist dimensions between −0.5 to 0.5 day, and −1 to 1° relative to the given box).

We use this strategy to capture the main variability of the ocean response and to avoid potential biasing caused by the un-even distribution of Argo pairs in space and time. Key points of this methodology include: (1) categorizing the events into weak and strong events/conditions, and (2) focusing on the cross-track temperature response, using a footprint technique that averages along storm tracks and thus neglects along-track variability. Point 2 reflects the assumption about the importance of the asymmetric cross-track thermal response compared to along-track directions, which has been noted in numerous previous case studies (Black and Dickey, 2008; Deal, 2011; Price et al., 2008). However, recent studies (Jaimes and Shay, 2010; James et al., 2011) suggest ocean variability along the track can substantially modulate the ocean cooling response to TC forcing and distort the temperature anomaly in the wake of the storm, which can be important within western boundary currents and associated geostrophic vortices. As a first step to determine TC effects on upper ocean thermal structure on a global scale, we focus primarily on the cross-track ocean response, and we average along the storms' translational direction of motion.

As state previously, our methodology requires the distance between two Argo profiles in a pair to be less than 0.2°. However, we do not require the pre-storm and post-storm measurements to be recorded from the same float. This criterion is in contrast to recent regional analysis using Argo data (Park et al., 2011), who stipulated the constraints that: two profiles are to be measured by the same Argo float in order to reduce the float-to-float calibration difference, and the maximum distance between measurements to be less than 200 km. In the current study, ∼ 80 % of the pre-storm and post-storm measurements are from the same float.

Figure 1 shows the geographical distribution of the TC tracks along with all of the Argo pairs from January 2004 to December 2012, highlighting the global coverage of

OSD
11, 2831–2878, 2014

the Argo pairs in TC-affected regions (4410 total pairs). Tropical cyclones have preferred locations and directions of motion. For example TCs in the northwestern Pacific move to the northwest between 10–20° N and northeast between 20–40° N. This preferred storm location and direction of motion results in coastal pairs in the northwestern Pacific located on the left side of tracks, while the pairs away from the coast are typically located on the right side of the tracks. In the northeastern Pacific, TCs generally move to the northwest, leading to a clear distribution of right-side pairs in 20–40° N and left-side pairs in 0–20° N. Similarly, in the north Atlantic, the distribution of TCs leads to the left-side pairs mainly distributed between 0–15 and 40–50° N. But in the Indian and Southern Pacific Ocean, the left and right side pairs mix together. These preferred locations of TCs and the resulting distributions of Argo pairs (Fig. 2) can affect the geographical pattern of the TC-induced oceanic response.

The distributions of Argo pairs are presented in Fig. 3 for the category, observation time (relative to storm passage), depth, and distance from storm center. Figure 3 reflects several key features of the methods and analysis, including: (1) the uneven distribution of the data, (2) the larger number of Argo pairs for the TS/TD conditions than Hurricanes (TS/TD conditions are much more common), (3) the number of Argo pairs decreases with time (e.g. we sample more pairs between 0–10 days after storm passage compared to 10–20); and (4) we obtain the least number of pairs near storm centers. Point 4 may be due, in part, to unreliable Argo measurements associated with severe conditions near storm centers (bad profiles) and/or strong horizontal currents ($\sim 100\,\mathrm{cm\,s^{-1}}$) advecting the floats away from the storm centers. To check whether there are some systematical differences (i.e. drifting) of horizontal distance between the two profiles in a pair, we calculate the horizontal difference between the two profiles as in Appendix B. In both geographical coordinates and track coordinates, we find no significant effects of drifting.

The footprint method outlined above features several key methodological limitations, which include: (i) neglecting along-track TC-induced ocean variability by averaging along storm tracks, (ii) lack of Argo float comparisons within individual storms due

OSD
11, 2831–2878, 2014

to poor sampling at these spatial and temporal scales; and (iii) the effect of background ocean variability at specific sampled locations, which is difficult due to the sparseness of the floats and frequency of the measurements.

3 Estimation of background variability in Argo pairs

Isolating the TC-induced thermal changes using Argo floats is difficult, because biases can arise due to changes in the thermal structure of the background ocean state. These biases can be caused by many processes such as: the seasonal cycle, meso-scale signals and large-scale spatial variability. Here we employ a test to examine potential biases and quantify background errors related to our footprint method described in the previous sections. Background noise is estimated by using Argo pairs under quiescent conditions (i.e., without TCs), hereafter denoted as NoTC-pairs.

Our methodology for analyzing background variability is outlined in the following steps:

1. We collect all Argo profiles during January 2004–December 2012 for which there are no TCs within $\pm 8^{\circ}$ distance of their location and -50 to $+5$ days relative to storm passage. These profiles are denoted as NoTC-profiles.

2. Background Argo pairs are formed by using these NoTC-profiles. The sampling strategy is the same as the TC pairs. One Argo pair consists of two Argo profiles, which are within 0.2° and 20 days. 20 days is set here to make this time scale comparable with the time scale of the typical TC response. We tested the sensitivity of the analysis to the choice of time scale, by also analyzing variability out to 40 days. The results were consistent for both time scales.

3. The pairs are then spatially and temporally chosen according to TC track and TC-affected pairs. In each 4° by 8° grid box and 1 month time period during each year, if there is at least one TC-affected pair, background pairs detected in step 2 are

flagged as "legal-NoTCpair" and all of the un-flagged pairs are removed. By using this strategy, all of the remaining pairs (NoTC-pairs) are comparable to the TC-affected pairs for all locations and dates. Thus for each storm track, background pairs are collected across all years corresponding to storm track locations and timing of events (within a given year). This sampling strategy provides a consistent method for analyzing background variability, by comparing Argo pairs from the same regions and times of year during storm (TC-pairs) and non-storm (NoTC-pairs) conditions.

4. To frame the background signals into the context of our footprint method, the NoTC-pairs obtained in step 3 are converted to a background footprint (denoted as NoTC-TSTD-footprint and NoTC-Hur-footprint for TS/TD and Hurricane respectively). To summarize the method, each TC-footprint bin, for example F_{TSTD} with a bin denoted by (dist, depth, δt), contains n TC-affected pairs with geographical locations of (lat_i, lon_i) $i = 1 : n$. The NoTC-TSTD-footprint (NoTC-Hur-footprint) at the same bin (dist, depth, δt) is calculated by selecting m NoTC-pairs according to the locations of TC-affected pairs. If there exists a NoTC-pair within 2° to (lat_i, lon_i), this NoTC-pair is selected to calculate the NoTC-TSTD-footprint(dist, depth, δt) (NoTC-Hur-footprint(dist, depth, δt)). In the construction of the background footprint, m is set to n. In this case, we define background variability at a single location in terms of one NoTC-pair. Using one NoTC pairs corresponding to a given TC pair enables strict comparison between the two data sets. Otherwise, the method will yield more weight to individual pairs from locations with low TC activity (e.g. where there are many NoTC pairs compared to TC pairs). However, we have performed additional tests using all of the pairs from step 3, and the results are generally consistent with the constraints employed here.

By using the background pairs selected as above, both the NoTC-TSTD-footprint and NoTC-Hur-footprint are obtained according to the footprint method proposed in the previous section. In this case, the background signals can be directly comparable to the TC footprint (F_{TSTD} and F_{Hur}).

In total, 13 701 pairs are collected after step 3 is conducted. All the Argo profiles are under the same quality control procedures as the TC-affected Argo profiles discussed in the previous section. Figure 4a and b displays the total amount of TC-pairs and NoTC-pairs in each 4 by 8° degree grid boxes. The spatial distribution of NoTC-pairs is generally consistent with the TC-affected pairs.

The errors and biases due to the presence of background variability are quantified using two independent methods described in the following subsections. We first conduct a gross check on background error (described in Sect. 3.1), and we quantify the background error using the footprint method (described in Sect. 3.2).

3.1 Gross check

By applying a gross check, we are aiming to check the magnitude of the global-averaged background signals and the size of the background uncertainties in TC-affected regions and seasons. We also compare the error with standard Argo accuracy of ~0.005 °C. We define the temperature differences of these NoTC-pairs as background noise (dBT_a) using the functional form:

$$\mathrm{dBT}_a = \mathrm{dBT}_a(\mathrm{time}, \delta t, \mathrm{depth}, \mathrm{lat}, \mathrm{lon})$$

where time denotes the Julian day of the reference Argo profile; δt is the time difference between the two Argo profiles in each pair; lat and lon denote the spatial locations of a pair; and depth is the depth of a temperature anomaly. These anomalies are collected in two maps to test for any systematical temporal or spatial biases in background pairs:

$$\text{Back-Map1 (depth)} = \int_{\mathrm{day1}}^{\mathrm{day}_2}\int_{\delta t_1}^{\delta t_n}\int_{\mathrm{lat1}}^{\mathrm{lat2}}\int_{\mathrm{lon1}}^{\mathrm{lon2}} \mathrm{d}T_{a_1}(\mathrm{day}, \delta t, \mathrm{depth}, \mathrm{lat}, \mathrm{lon}) d_{\mathrm{lon}} d_{\mathrm{lat}} d_{\delta t} d_{\mathrm{day}} / n(\mathrm{depth})$$

OSD
11, 2831–2878, 2014

Back-Map2 $(\delta t) =$

$$\int_{\text{day1}}^{\text{day}_2}\int_{\text{depth}_1}^{\text{depth}_n}\int_{\text{lat1}}^{\text{lat2}}\int_{\text{lon1}}^{\text{lon2}} \mathrm{d}T_{a_1}(\text{day}, \delta t, \text{depth, lat, lon}) d_{\text{lon}} d_{\text{lat}} d_{\text{depth}} d_{\text{day}} / n(\delta t)$$

where n (depth) and $n(\delta t)$ denote the number of pairs for each depth and each δt respectively. In Back-Map1, all of the background temperature anomalies are grouped into bins representing 5 m thickness between 0 to 2000 m depth. In Back-Map2, temperature anomalies are grouped into temporal bins of size 0.5 days between 0 and 20 days.

The mean and ±1 SD of the background noise as a function of depth and δt are presented in Fig. 5. The means of the background noise with depth are near zero with a very small positive temperature anomaly near the sea surface (20–100 m with the peak about 0.005 °C), which may be caused by seasonal/meso-scale signals. However, this anomaly is negligible compared to TC signals (discussed in the following sections).

The means of the background variability as a function of time also show no trend with δt (Fig. 5b) for 0–1000 m (also no trend for 0–20 m, not shown here). The 0–1000 m averaged standard deviations of Argo pairs influenced by Hurricanes and TS/TD show a 0.1–0.2 °C larger deviation compared to estimates of background variability, which shows that TCs can disturb normal ocean conditions and that the perturbation is observable using this methodological framework.

Next, we apply a bootstrap analysis to determine the effect of sample size on characterizing potential biases, errors, and background variability. At each depth, we randomly choose a certain number of pairs (the number of samples changes from 10 to 9000, with a step size of 20), and we calculate the mean of the temperature anomalies of the chosen pairs. This procedure is repeated 200 times yielding 200 means, and we calculate the standard deviation of the 200 means at each vertical level. Figure 6a shows the standard error at different depths against sample sizes, indicating the error of the temperature anomalies decrease with sample size. When sample sizes are greater

OSD
11, 2831–2878, 2014

than 400, the standard error at depths deeper than 400 m is less than 0.02 °C. and at depths less than 400 m the standard error is less than 0.06 °C. Both of these errors are less than 5 % of standard deviations at corresponding depths shown in Fig. 6a. When the sample size is increased, the error is gradually reduced and converges near the Argo sensor accuracy (0.005 °C) for the upper shallow depths and below the Argo sensor accuracy for deeper levels. This result suggests that increasing the amount data generally reduces the background error when averaged over large areas.

We consider the time evolution of background noise by randomly choosing a specific number of pairs (the number changes from 10 to 900, with a bin size of 20) and calculate the mean of the selected samples. This procedure is also repeated 200 times, and then we calculate the standard deviation of the 200 time means. Figure 6b shows the standard error for different times as a function of sample sizes, showing a consistent error at different times in general. For sample sizes greater than 200, the standard error is generally less than 5 % of the standard deviations shown in Fig. 6b (e.g. less than 0.03 °C for all time differences). Considering that the Argo accuracy is ∼ 0.005 °C, the error we detected is several times larger than the Argo accuracy.

3.2 Background footprint

To be consistent with our method for quantifying TC-induced ocean thermal changes, we construct a similar footprint that is a composite based on background pairs. NoTC-TSTD-footprint and NoTC-Hur-footprint is presented for two time periods: 0–3 days and 4–20 days for TS/TD and Hurricane respectively (Fig. 7). For TS/TD locations, the background thermal anomalies for the two time periods show no clear pattern at any depths or spatial locations across the track. Since these background pairs are selected according to the dates and locations of TC-affected pairs but in different years, we conclude that the footprint method produces no significant background patterns.

The standard deviations of the NoTC-TSTD-footprint and NoTC-Hur-footprint is presented in Fig. 8, corresponding to the mean of background footprints shown in Fig. 7. It appears that the standard deviations (SD) show a similar vertical distribution for the two time periods and storm categories. In the upper 20 m, typical SD values are around 0.4 °C. From 20–200 m, we find larger SD values between ∼ 0.6 and 1.2 °C, and SD decreases below 200 m. The background SDs for TS/TD locations show larger values below the surface (20–200 m) than for hurricane locations. However, none of these figures show a systematical distribution of SDs across the storm track, thus suggesting again no substantial background biases. We detect a slight bias along the left side of the storm tracks within background SD for both TS/TD and Hurricane locations, which may be due in part to the presence of more coastal pairs on the left side of TC tracks in high activity TC regions.

These tests of the background variability show that background errors are generally small at all depths considered here (between 0 and 2000 m) and time scales (between 0 ∼ 20 days) compared to the TC signals (discussed in the following sections), and we find no significant background biases using the footprint strategy. We will use these results as the basis (i.e. null hypothesis) for testing the significance of the observed TC effects in the following section.

4 Results and discussion

Here we present the 3-Dimensional footprint maps for two time intervals, 0–3 days and 4–20 days referenced to storm passage. The 0–3 day interval represents about two inertial periods and reflects the direct ocean response to storm forcing (Sanford et al., 2011). We choose 3 days as an upper limit to the forced stage based on the following methodological constraints, limitations and uncertainties: (1) TC track information is every 6–12 h, and Argo data may be offset by several hours due to its ascent speed; together these effects can lead to observational offsets up to 1 day; and (2) the inertial period changes rapidly with latitude in TC-affected regions (from 1 to 3 days). Considering these uncertainties, we choose 3 days as an approximation on the forced stage on the global scale, which represents the initial period of the TCs' influence on upper-ocean properties. We have conducted additional sensitivity tests to the choice of forced

Discussion Paper | Discussion Paper | Discussion Paper | Discussion Paper |

OSD

11, 2831–2878, 2014

Global representation of tropical cyclone-induced ocean thermal changes

L. Cheng et al.

stage time interval using −1 to 2 days relative to storm passage, and the results are generally consistent to what we show here.

After 4 days, the ocean typically begins recovering to pre-storm and/or climatological conditions. While this restoration period can persist from weeks to months (Mei et al., 2013; Mei and Pasquero, 2013), this analysis averages the thermal response between 4 and 20 days after storm passage to estimate the mean ocean response during the recovery stage. Anomalies for both forced and recovery stages are referenced to pre-storm conditions as discussed in the methods section.

The amount of data for each footprint composite for the two time periods is shown in Fig. 9. In the upper 100 m, the number of measurements is generally more than 30 in each 0.5° box except near the storm center. The measurements generally decrease with depth especially deeper than 1000, 1200 and 1500 m (parking depths).

4.1 0–3 days footprint of ocean thermal changes

During storm passage, in the so-called forcing stage (Price et al., 1994), the cyclonic winds generally pump cold water up to the surface near the storm eye (Ekman pumping) and generate divergent currents in the upper ocean. To compensate the upwelling, down-welling away from the track occurs over a large area, appearing as ocean warming in the subsurface regions. The upwelling and down-welling oscillate with a near-inertial period (Price, 1983), which has been termed "inertial pumping" (Shay et al., 1998). Meanwhile, the strong and sudden disturbance of storm winds generates near-inertial horizontal currents (Shay and Elsberry, 1987), which have both horizontal and vertical velocity shear, leading to cold-water entrainment at the base of the mixed layer.

The detailed vertical structure of ocean interior responses to hurricanes and TS/TDs are presented in Fig. 10a and c, where the significant signals are isolated compared with background variations. The standard errors are shown in Fig. 10b and d. Figure 10 shows that both hurricanes and TS/TDs induce an asymmetric sea surface cooling with pronounced cooling on the right side of the track (in track coordinates). A much weaker pattern is found on the opposite side, supporting the asymmetry of the ocean response documented previously in the literature. These near surface cooling signals have uncertainties (standard errors in Fig. 10b and d) with magnitudes of less than 40 % of the signals. The rightward-biased cooling in the track coordinate system near the surface is also found in previous studies to be due to the turning of the wind stress vector with storm passage, which is the same direction as inertial oscillations on the right side of the storms in the Northern Hemisphere (left side in the Southern Hemisphere) (Dare and McBride, 2011; Price, 1981; Sanford et al., 2011). TC winds are stronger on the side of the storm where the translation speed of the storm and the wind vector itself are acting along the same direction; this effect is less along the left side of the storm. Near-inertial dynamics of these forced currents driven by wind stress determines the strength of the vertical shear that can eventually produce instability, mixing and cooling near the surface. This vertical shear triggers more mixing on the right side in track coordinates, thus inducing more cooling through entrainment (Dickey et al., 1998; Price, 1983). This mechanism contributes ~ 80 % of the SST response (Price et al., 1994). Another cooling mechanism is due to the turbulence generated also by wind stress (Chan and Kepert, 2010). Both are irreversible processes that produce mixed layer deepening. The mixing transports heat vertically from sea surface to the subsurface, appearing a subsurface warming corresponding to the near-surface cooling, which is apparent in Fig. 10 with a peak at ~ 50–100 m.

Figure 10 shows a subsurface (30–200 m) cooling within 1° of the track, and a subsurface warming on the both sides of the track between ±2 to 4° from the storm center. These warming signals contain relatively large uncertainties (the standard error ranges from 40 to 100 % of the absolute value of the signals) compared with surface signals, partly because they occur within the thermocline which exhibits higher variability. Our composite analysis of the response from Argo floats confirms that there is a Ekman solution in the upper ocean (upper 200 m), in that we observe a residual vertical motion within 1° of the storm track, appearing as a net column-averaged cooling near the storm center, along with down-welling outside the storm center according (Fig. 10a and b). It is also possible that instantaneous wind erosion plays a role in addition to

OSD
11, 2831–2878, 2014

upwelling (Jacob and Shay, 2003; James et al., 2011) for the upper ocean changes (upper 200 m), in particular during slower storms that produce weaker near-inertial velocity responses. Despite smoothing out of inertial oscillations, the resultant subsurface warming is observable.

At depths greater than 200 m, we find a weak cooling signal near the storm center and weak warming away from the storm. The weak cooling near the storm center (between −1 and +1°) is significant down to 400 m for hurricanes and 200 m for TS/TD. These signals have large uncertainties, with standard errors up to 100 % of the signals (Fig. 10d). The causes for these deep ocean responses cannot be fully answered using this methodology, however, geostrophic adjustment may be one physical mechanism. Comparison of the TC thermal response with background oceanic variability indicates that the major structure of TC-induced thermal changes is significant compared with the background variability, as highlighted by black lines in Fig. 10a and c.

The cross-track footprint of the oceanic thermal response is averaged over depth (0–1200 m) during days 0–3 days relative to storm passage (Fig. 11), and we highlight the different characteristics of the response of the upper ocean (0–20 m) vs. the entire column depth. Near the surface (0–20 m), for hurricanes, the cooling spreads to a large area of ±5° from the storm center with a peak around ∼ −1.1 °C. In contrast, for TS/TD, we observe less cooling over a smaller area (a peak of ∼ −0.5 °C). The sea surface anomalies estimated by Argo observations are consistent with other SST observations presented by multiple previous studies (Lloyd and Vecchi, 2010, 2011; Mei and Pasquero, 2013)

For the response of the entire ocean column, TS/TD generally cause cooling between −1 and +3° in storm coordinates, implying that the dominant mechanism affecting column-integrated temperature changes in TS/TD-affected regions is surface fluxes. The wind-driven entrainment itself does not change the ocean heat content of the whole water column, instead re-distributing the heat vertically via mixing. Ocean currents also advect mass and heat from its origin to different locations but do not change the net ocean heat content. Therefore, if there is a net ocean heat content

OSD
11, 2831–2878, 2014

change over TC-affected region, it must be via the surface heat flux which exchanges heat between the ocean and atmosphere. A significant heat flux is also found in previous studies (Bell et al., 2012; Lin et al., 2009b; Mcphaden, 2009), and additional analysis of the role of air–sea heat fluxes will be presented in a separate study.

For hurricanes, the water column experiences a cooling within ±2° of storm center, and stronger warming near between +2 and +4° along the right side of the track (in track coordinates). Both cold and warm peaks are significant at the 90 % confidence level according to the Null-hypotheses tests (Appendix A). This implies that there is a net heat transport from the storm center to the right side of the storm relative to the storm's direction of motion. The magnitude of column-averaged cooling (within +2° of the storm center) is greater than the warming along the right side (+2 ~ 4°), thus the net effect is a cooling of the upper ocean through enhanced surfaces fluxes.

4.2 4–20 days footprint of ocean thermal changes

After storm passage, radiative forcing and ocean currents tend to restore the storm-induced surface anomalies. Past studies show that upper-ocean thermal anomalies can persist on the order of: 10–20 days (Price et al., 2008), 20–30 days (Dare and McBride, 2011), or even longer than 30 days (Mei et al., 2013; Mei and Pasquero, 2013; Park et al., 2011). Differences in timescales likely depend on differences in regional and seasonal ocean conditions (i.e. when and where TCs occur). Surface cooling is typically restored within 20 days according to satellite observations (Hart et al., 2007a), while thermal effects within the ocean interior may persist on inter-seasonal timescales (Jansen et al., 2010; Park et al., 2011). The mechanical energy is dispersed by continuous mixing near the surface and within the thermocline, as well as propagating internal waves to the larger ocean basin (Shay et al., 1989), with a delay of about 5–10 days (Price et al., 1983).

The vertical structure of the general temperature response between 4 and 20 days after storm passage, relative to pre-storm conditions, is shown in Fig. 12. Weak cooling still dominates the subsurface (100–200 m) response near the storm center. But the standard error can be 100–150 % of the signal, maybe because of the longer time window (17 days in total). This weaker subsurface cold anomaly compared with the 0–3 days response implies that cooling caused by upwelling is going to be restored on timescales of 20 days, and this signal may be associated with the geostrophic ridge that develops in the wake of storm following the dispersion of near-inertial waves (Geisler, 1970). In addition, the near-surface cold anomaly along the right-side of the storm is still apparent during this restoration stage, thus pointing to the persistence of the TC signal.

Figure 12 shows persistent warm anomalies between 20 and 200 m along both the right and left sides of the storm tracks, which are greater in magnitude than the observed forced stage response (0–3 days), with typical standard error (as a percentage of the TC signal) of 30–70 % for TS/TDs and 30–90 % for Hurricanes. It is likely that near-inertial current shear promotes enhanced mixing for several inertial cycles after storm passage, thus providing a mechanism for vertical mixing and heat convergence for days-to-weeks after storm passage. Another possible reason for this stronger subsurface warming anomaly is due to horizontal advection by large-scale ocean currents, such as intense western boundary currents which can potentially transport heat into TC regions on the considered timescales. However, we do not find similar temperature anomaly structures in the background variability for high TC activity basins (e.g. west Pacific), even when extending the background pairs selection criteria to 40 days and 60 days (figures not shown). It may also be possible that TCs directly affect the boundary current structure, such that there is warm advection into the TC-affected regions after storm passage as the boundary current returns to its climatological (or pre-storm) state. In this case, our methodology prohibits analyzing direct effects of TCs on the background state, since TCs and background variability are examined separately from different sets of Argo pairs. Thus, any potential dynamical connections between TC forcing and the large-scale currents are beyond the scope of this study.

Figure 13 shows the vertical profile of the spatially averaged (−6 to +6°) thermal response during the TC recovery stage relative to pre-storm conditions. We find vertical mixing and upwelling/downwelling induces significant cooling near the surface (0–20 m depth) and subsurface warming within the upper thermocline (50–200 m) for both TS/TD and hurricanes. The signals deeper than 200 m exhibit relatively weak cooling, and they are only significant for Hurricanes near the storm center. As noted by previous studies, deep ocean (below 400 m) thermal responses are rarely observed. One observation down to 530 m (Price, 1981) shows a large oscillation with amplitude about 30 m at the depth of 530 m after 10 days of storm passage. A study using a mooring observation (Brink, 1989) observed a TC-induced temperature oscillation at depths around 1000 m. Because of the lack of observations, further observational and theoretical studies are needed to understand the response of the interior ocean to extreme surface wind forcing below 200 m.

5 Caveats

The methodology presented here contains several key caveats and limitations. One outstanding question relates to the accuracy of the no-TC pairs in capturing the interannual variability in the timing of events. In other words, given that years with tropical cyclones are likely to have different positioning/intensity of major atmospheric circulation patterns such as subtropical highs, one could expect to see a Rossby wave response from such shifts resulting in potentially anomalous trends at depth. To address this issue, we conducted the following test:

TC-affected pairs are subdivided into two subsets: one contains data from 2004–2008 and the other from 2009–2012. We subdivide storms to analyze sensitivity of our footprint results to different spatial patterns of storm locations. The results for TS/TD and Hurricane 4–20 days footprints are presented in Fig. 14, both compared with the 2004–2012 results in black contours. In the figure, the main pattern is similar for the two time periods, with only some strength differences of the signals. In addition to this test, we calculate footprints of the background pairs for the two periods (not shown), and the differences are within the limit of insignificant noise. Results support the notion

OSD
11, 2831–2878, 2014

that the background signals can be mostly smoothed out by using footprint strategy when averaging over large amounts of data with variant time and spatial distributions.

An additional caveat relates to vertically propagating waves forced by the storms. For example, mooring data has shown evidence of vertically propagating Rossby waves. Unfortunately, our method may not be able to distinguish the effects of these evanescent waves due to the following: (i) these non-permanent signals may be filtered by averaging a large amount of data over a long period of time, and (ii) we do not observe any such wave structure or patterns in our analysis (such as thermal anomaly across track in Figs. 10 and 12). However, the potential effect of vertical propagating waves on upper-ocean temperature and energy budgets remains an active area of research (Ascani et al., 2010; Sriver et al., 2013).

Ocean stratification varies regionally, which can in turn pose problems for estimating global averages of ocean responses to TCs. To quantify the effect of regional variability, we calculate TC-induced ocean thermal changes within 4–20 days within three ocean basins separately: Pacific Ocean, Indian Ocean and Atlantic Ocean. Note, we also subdivide the Pacific basin into separate regions – Western/Eastern/Southern Pacific). Figure 15 shows the results in the footprint composite format. Key findings include: (i) the global-averaged thermal footprint pattern (Fig. 12c) is generally consistent with the pattern in Pacific Ocean, especially in Western Pacific (Fig. 15a and d), since there are ~ 2500 pairs from the Pacific Ocean (or roughly ~ 60 % of the total number of pairs globally); and (ii) although the footprint within the Atlantic and Indian Oceans have large uncertainties, key characteristics of the general patterns are robust, such as ocean cooling near the storm center from surface to subsurface (0–200 m) and subsurface warming along both sides of the track (Fig. 15e and f). However, only 25 and 15 % of the Argo pairs globally are sampled from the Indian Ocean and Atlantic Ocean respectively, thus physical interpretations are limited by the relative lack of data. (iii) In the Eastern Pacific, the ocean responses seems to be different from other regions, which appears cooling at the left side of TC as shown in Fig. 15b. This difference may be due to the

OSD
11, 2831–2878, 2014

lack of data in this region, indicating that our method is insufficient to reconstruct the local responses to TCs.

6 Conclusions

We use Argo data to create a global representation of TC-induced changes in upper ocean temperature, using a new footprint method to create a composite analysis of the vertical profile of the cross-track ocean temperature response for two distinct time scales (0–3 days and 4–20 days relative to storm passage) and categories (TS/TD and hurricanes), and we include all TCs occurring globally from 2004–2012. We find this method is capable of capturing the main characteristics of TC-induced ocean variability related to cross-track and intensity variations, as well as the differences in the response due to the choice of time scales (e.g. forcing vs. recovery).

Our findings indicate that during the interval 0–3 days, weak storms (categorized TS/TD) show a column-averaged cooling over the TC-affected region, while strong storms (categorized hurricanes) show a column-averaged cooling near storm center but a net warming along the right side of the storm track (in a storm referenced coordinate system) within 2–4° from storm center. We attribute these changes to the combination of effects from upwelling and downwelling, divergent and convergent currents, vertical mixing, and enhanced air–sea surface fluxes during storm passage. The other prominent feature of TC effects is subsurface warming for both TS/TD and hurricanes, which is possibly induced by mixing (entrainment) and downwelling. Strong storms induce stronger and deeper subsurface responses than the weak storms. Furthermore, the typical asymmetric cooling response at the sea surface is observable for both TS/TD and hurricane conditions, consistent with previous studies. In addition to the near-surface response, we analyze the vertical temperature profiles to 1200 m depth within TC-affected regions. We find that both TS/TD and hurricanes induce, on average, significant ocean subsurface warming between 100 and 200 m depth. Net

OSD
11, 2831–2878, 2014

cooling is observed between 200 and 500 m for both TS/TD and hurricane conditions, but the response is statistically significant only for Hurricane conditions.

In this study, the estimation of TC-induced ocean thermal changes presented can improve our understanding of potential climate feedbacks associated with TC activity. These feedbacks may impact ocean (Fedorov et al., 2010; Sriver et al., 2010) and atmospheric circulations (Hart, 2011). The global network of Argo profiles is a powerful tool to observe ocean conditions under TCs. Additional applications of the methodology outlined here include: analysis of air–sea heat fluxes during and following TCs, estimation of vertical redistribution of ocean heat and heat convergence, and process-oriented studies on TC forcing and upper ocean responses. In a companion paper to this study, we will apply the techniques developed here to quantify global air–sea heat fluxes and changes in ocean heat content attributable to TC forcing.

Appendix A: Null-hypothesis test on Argo data

Here we present a null-hypothesis test to analyze whether the proposed footprint method is capable of capturing the tropical cyclone signals compared to the background variability. Our hypothesis is that the detected TC signals are significant compared to background noise. The null-hypothesis is that the TC-induced signal is the average of background noise (H_0: $\mu = B$, where B is the mean of background noise). The alternative hypothesis claims TC-induced signals are either higher or lower than the average of the background noise (H_1: $\mu \neq B$).

A two-sided z test is conducted to test the hypothesis. Sampling distributions of the means (SDM) are used to assist in analyzing the results. Assuming the null-hypothesis is true, the sampling distribution of TC-induced signals (denoted as "x") based on sample counts (denoted as "n") will be normally distributed with a mean of background mean (B) and standard error of ($\sigma/\sqrt{n}$), where σ is the standard deviation of background noise. Therefore, under hypothesis H_0, the observed "x" should be: $x - N(u, \sigma/\sqrt{n})$. We want to find an interval (x^-, x^+) for x, which would lead to the acceptance of the null hypothesis. To meet this need, we calculate: $x^+ = z_{stat} \cdot \text{SEM} + B$ and $x^- = -z_{stat} \cdot \text{SEM} + B$, where z_{stat} quantifies how far x is from B in standard deviation units. Here the value of z_{stat} corresponds to a probability threshold (or p value) of 0.05. The value of 0.05 means the observed signals is "highly significant" within 95 % confidence interval, if they are outside the interval of (x^-, x^+). SEM is the standard error $(\sigma/\sqrt{n})$.

Based on this strategy, we calculate the "highly significant" intervals for temperature anomalies as a function of depth and distance respectively (shades in Figs. 11 and 13), and for the footprint (thick solid contours in Figs. 10 and 12). In brief, the confidence interval in Figs. 10 and 12 is calculated by $x^+ = z_{stat} \cdot \text{SEM} + B$ and $x^- = -z_{stat} \cdot \text{SEM} + B$ at each grid box. σ is the standard deviation of background noise calculated in Fig. 8, and the background mean (B) is shown in Fig. 7. Sample counts n is the number of TC-pairs at each grid box.

To obtain confidence intervals for Figs. 11 and 13, the mean (B) and standard deviation (σ) of background noise with time and depth are calculated as in Fig. 5. While those for distance are set manually based on the notion that the background noise is confirmed to be white noise. The background mean with distance is set to zero, and the standard deviation is set to the mean of standard deviations at the first 3 days.

Appendix B: Test on the horizontal distances of the two Argo floats in a pair

In this study, 0.2° is selected as the maximum horizontal distance between the reference-Argo and TC-affected Argo, since evidence suggests this choice will minimize the influences of the strong background signals (such as meso-scale eddys, strong Kuroshio, Califonia Currents, and internal waves). Ideally our footprint strategy aims to detect the ocean thermal changes at a fixed position. But to obtain a satisfied amount of pairs, the 0.2° criteria is used, thus there is the potential for sampling biases associated with horizontal and vertical motions on upper ocean currents. Therefore,

OSD
11, 2831–2878, 2014

it is necessary to test whether the selection of pairs within 0.2° influences our main results.

Here we compare the position of floats before and after storms from each TC-affected pair by using two coordinate systems. This test is conducted for Same-float pairs (i.e. the two profiles in a pair are both measured by the same float) and Different-float pairs separately (i.e. the two profiles in a pair are measured by two different floats). One test uses latitude–longitude (Fig. A1a), and the other test uses track coordinates (Fig. A1b), and both coordinate systems use the location of the float before the storm as the origin. The post-storm float position appears to be randomly distributed around the initial pre-storm position. We examine the drifting direction along and across the track at different distances from the float to the track center, where the distance between pre-storm and post-storm Argo is calculated in track coordinates. Figure A2 shows that floats drift moderately but systematically in the water under forces of TCs, and a float tends to move away from the storm track (Pink), and move backward along the storm track (Red). However, we cannot explain these movements using the current methods, due to dynamical effects such as: surface wind forcing, near-inertial currents, and mean currents at Argo parking depths. But we find no systematical drift distance for Different-float-pairs. Since the maximum systematical drift within 20 days is less than 5 km, this distance is relatively small compared to the maximum displacement distance of 20 km. Therefore, we assume horizontal motions of the floats do not affect our essential results. Approximately, 17 % of pairs used in our analysis are considered Different-float-pairs.

Furthermore, it is worth noting Argo profiles affected by TCs may potentially be labeled as poor quality data in the Delayed Mode Quality Control process (Yu et al., 2010), since data is typically rejected if there are dramatic changes in temperature or salinity profiles. In this study we include the real-time Argo profiles as well as the delayed-mode data. However, we do not attempt to recover wrongly labeled data.

Acknowledgements. This work is supported by the project "Structures, Variability and Climatic Impacts of Ocean Circulation and Warm Pool in the Tropical Pacific Ocean" of National Ba-

OSD
11, 2831–2878, 2014

sic Research Program of China (Grant No.2012CB417404) and Chinese Academy Sciences' Project "Western Pacific Ocean System: Structure, Dynamics and Consequences" (Grant No. XDA10010405).

References

Ascani, F., Firing, E., Dutrieux, P., McCreary, J. P., and Ishida, A.: Deep equatorial ocean circulation induced by a forced-dissipated Yanai beam, J. Phys. Oceanogr., 40, 1118–1142, 2010.

Bell, M. M., Montgomery, M. T., and Emanuel, K. A.: Air–sea enthalpy and momentum exchange at major hurricane wind speeds observed during CBLAST, J. Atmos. Sci., 69, 3197–3222, doi:10.1175/jas-d-11-0276.1, 2012.

Black, W. J. and Dickey, T. D.: Observations and analyses of upper ocean responses to tropical storms and hurricanes in the vicinity of Bermuda, J. Geophys. Res.-Oceans, 113, C08009, doi:10.1029/2007JC004358, 2008.

Brink, K. H.: Observations of the response of thermocline currents to a hurricane, J. Phys. Oceanogr., 19, 1017–1022, 1989.

Camargo, S. J. and Sobel, A. H.: Western North Pacific tropical cyclone intensity and ENSO, J. Climate, 18, 2996–3006, 2005.

Chan, J. C. and Kepert, J. D.: Global Perspectives on Tropical Cyclones: from Science to Mitigation, Vol. 4, World Scientific Publishing Company, 94., 2010.

Cione, J. J. and Uhlhorn, E. W.: Sea surface temperature variability in hurricanes: implications with respect to intensity change, Mon. Weather Rev., 131, 1783–1796, 2003.

Dare, R. A. and McBride, J. L.: Sea surface temperature response to tropical cyclones, Mon. Weather Rev., 139, 3798–3808, 2011.

Deal, R.: Surface heating and restratification of the ocean after a tropical cyclone, Electronic Theses, Treatises and Dissertations, Paper 60, 2011.

Dickey, T., Frye, D., McNeil, J., Manov, D., Nelson, N., Sigurdson, D., Jannasch, H., Siegel, D., Michaels, T., and Johnson, R.: Upper-Ocean Temperature Response to Hurricane Felix as Measured by the Bermuda Testbed Mooring, Mon. Weather Rev., 126, 1195–1201, 1998.

Emanuel, K.: Contribution of tropical cyclones to meridional heat transport by the oceans, J. Geophys. Res.-Atmos., 106, 14771–14781, 2001.

Fedorov, A. V., Brierley, C. M., and Emanuel, K.: Tropical cyclones and permanent El Nino in the early Pliocene epoch, Nature, 463, 1066–1084, 2010.
Freeland, H., Roemmich, D., Garzoli, S., LeTraon, P., Ravichandran, M., Riser, S., Thierry, V., Wijffels, S., Belbéoch, M., Gould, J., Grant, F., Ignazewski, M., King, B., Klein, B., Mork, K., Owens, B., Pouliquen, S., Sterl, A., Suga, T., Suk, M., Sutton, P., Troisi, A., Vélez-Belchi, P., and Xu, J.: Argo – a decade of progress, in: Proceedings of OceanObs'09: Sustained Ocean Observations and Information for Society Venice, Italy, 21–25 September 2009, edited by: Hall, J., Harrison, D. E., and Stammer, D., ESA Publication WPP-306, 2009.
Geisler, J. E.: Linear theory of the response of a two layer ocean to a moving hurricane, Geophys. Astro. Fluid, 1, 249–272, 1970.
Ginis, I.: Tropical cyclone-ocean interactions. Atmosphere–ocean interactions, edited by: Perrie, W., Adv. Fluid Mech. Ser., 33, 83–114, 2002.
Hart, R. E.: An inverse relationship between aggregate Northern Hemisphere tropical cyclone activity and subsequent winter climate, Geophys. Res. Lett., 38, L01705, doi:10.1029/2010GL045612, 2011.
Hart, R. E., Bosart, L. F., and Hosler, C.: The possible seasonal climate impact from anomalous frequency of recurving tropical cyclones, in: Preprints, 19th Conf. on Climate Variability and Change, San Antonio, TX, Amer. Meteor. Soc., 6.3, 2007a.
Hart, R. E., Maue, R. N., and Watson, M. C.: Estimating local memory of tropical cyclones through MPI anomaly evolution, Mon. Weather Rev., 135, 3990–4005, 2007b.
Jacob, S. D. and Shay, L. K.: The role of oceanic mesoscale features on the tropical cyclone-induced mixed layer response: a case study, J. Phys. Oceanogr., 33, 649–676, 2003.
Jaimes, B. and Shay, L. K.: Near-inertial wave wake of hurricanes Katrina and Rita over mesoscale oceanic eddies, J. Phys. Oceanogr., 40, 1320–1337, 2010.
James, B., Shay, L. K., and Halliwell, G. R.: The response of quasigeostrophic oceanic vortices to tropical cyclone forcing, J. Phys. Oceanogr., 41, 1965–1985, 2011.
Jansen, M. F., Ferrari, R., and Mooring, T. A.: Seasonal vs. permanent thermocline warming by tropical cyclones, Geophys. Res. Lett., 37, L03602, doi:10.1029/2009GL041808, 2010.
Lin, I. I., Pun, I. F., and Wu, C. C.: Upper-ocean thermal structure and the western North Pacific category 5 typhoons. Part II: Dependence on translation speed, Mon. Weather Rev., 137, 3744–3757, 2009a.

Lin, I. I., Chen, C. H., Pun, I. F., Liu, W. T., and Wu, C. C.: Warm ocean anomaly, air sea fluxes, and the rapid intensification of tropical cyclone Nargis (2008), Geophys. Res. Lett., 36, L03817, doi:10.1029/2008GL035815, 2009b.

Liu, Z., Xu, J., Zhu, B., Sun, C., and Zhang, L.: The upper ocean response to tropical cyclones in the northwestern Pacific analyzed with Argo data, Chin. J. Oceanogr. Limnol., 25, 123–131, 2007.

Lloyd, I. D. and Vecchi, G. A.: Submonthly Indian Ocean cooling events and their interaction with large-scale conditions, J. Climate, 23, 700–716, 2010.

Lloyd, I. D. and Vecchi, G. A.: Observational evidence for oceanic controls on hurricane intensity, J. Climate, 24, 1138–1153, 2011.

Mcphaden, J. M., Foltz, G. R., Lee, T., Murty, V. S. N., Ravichandran, M., Vecchi, G. A., Vialard, J., Wiggert, J. D., and Yu, L.: Ocean–atmosphere interactions during cyclone Nargis, EOS T. Am. Geophys. Un., 90, 53–54, doi:10.1029/2009EO070001, 2009.

Mei, W. and Pasquero, C.: Spatial and temporal characterization of sea surface temperature response to tropical cyclones, J. Climate, 26, 3745–3765, 2013.

Mei, W., Primeau, F., McWilliams, J. C., and Pasquero, C.: Sea surface height evidence for long-term warming effects of tropical cyclones on the ocean, P. Natl. Acad. Sci. USA, 110, 15207–15210, 2013.

Park, J. J., Kwon, Y. O., and Price, J. F.: Argo array observation of ocean heat content changes induced by tropical cyclones in the north Pacific, J. Geophys. Res., 116, C12025, doi:10.1029/2011JC007165, 2011.

Price, J. F.: Upper ocean response to a hurricane, J. Phys. Oceanogr., 11, 153–175, 1981.

Price, J. F.: Internal wave wake of a moving storm. 1. Scales, energy budget and observations, J. Phys. Oceanogr., 13, 949–965, 1983.

Price, J. F., Sanford, T. B., and Forristall, G. Z.: Forced stage response to a moving hurricane, J. Phys. Oceanogr., 24, 233–260, 1994.

Price, J. F., Morzel, J., and Niiler, P. P.: Warming of SST in the cool wake of a moving hurricane, J. Geophys. Res.-Oceans, 113, C07010, doi:10.1029/2007JC004393, 2008.

Sanford, T. B., Price, J. F., and Girton, J. B.: Upper-ocean response to hurricane Frances (2004) observed by profiling EM-APEX floats, J. Phys. Oceanogr., 41, 1041–1056, 2011.

Shay, L. K. and Elsberry, R. L.: Near-inertial ocean current response to hurricane Frederic, J. Phys. Oceanogr., 17, 1249–1269, 1987.

OSD
11, 2831–2878, 2014

Shay, L. K., Elsberry, R. L., and Black, P. G.: Vertical structure of the ocean current response to a hurricane, J. Phys. Oceanogr., 19, 649–669, 1989.

Shay, L. K., Mariano, A. J., Jacob, S. D., and Ryan, E. H.: Mean and near-inertial ocean current response to hurricane Gilbert, J. Phys. Oceanogr., 28, 858–889, 1998.

Sriver, R. L. and Huber, M.: Observational evidence for an ocean heat pump induced by tropical cyclones, Nature, 447, 577–580, 2007.

Sriver, R. L., Goes, M., Mann, M. E., and Keller, K.: Climate response to tropical cyclone-induced ocean mixing in an Earth system model of intermediate complexity, J. Geophys. Res.-Oceans, 115, C10042, doi:10.1029/2010JC006106, 2010.

Sriver, R. L., Huber, M., and Chafik, L.: Excitation of equatorial Kelvin and Yanai waves by tropical cyclones in an ocean general circulation model, Earth Syst. Dynam., 4, 1–10, doi:10.5194/esd-4-1-2013, 2013.

Willis, J. K., Lyman, J. M., Johnson, G. C., and Gilson, J.: In situ data biases and recent ocean heat content variability, J. Atmos. Ocean. Tech., 26, 846–852, 2009.

Yu, T., Han, G. J., Guan, C. L., and Deng, Z. G.: Several important issues in salinity quality control of Argo float, Mar. Geod., 33, 424–436, 2010.

OSD

11, 2831–2878, 2014

Global representation of tropical cyclone-induced ocean thermal changes

L. Cheng et al.

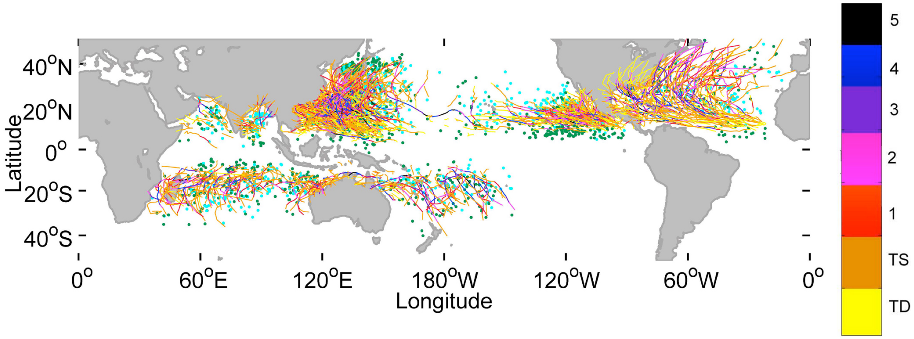

Figure 1. Tracks of tropical cyclones from January 2004 to December 2012, associated with the distribution of Argo pairs used in the paper. The colors of the tracks indicate the categories of tropical cyclone –tropical depression (TD; yellow), tropical storm (TS; orange), category 1–5 cyclones (denoted by red, magenta, purple blue, and black from category 1 to 5 respectively). The locations of Argo pairs are dotted in two colors: cyan dots are the pairs located at the right side of the corresponding TC-track, and green dots are the pairs located on the left side of the track. We analyze 885 tracks, and a total of 4410 Argo pairs.

OSD
11, 2831–2878, 2014

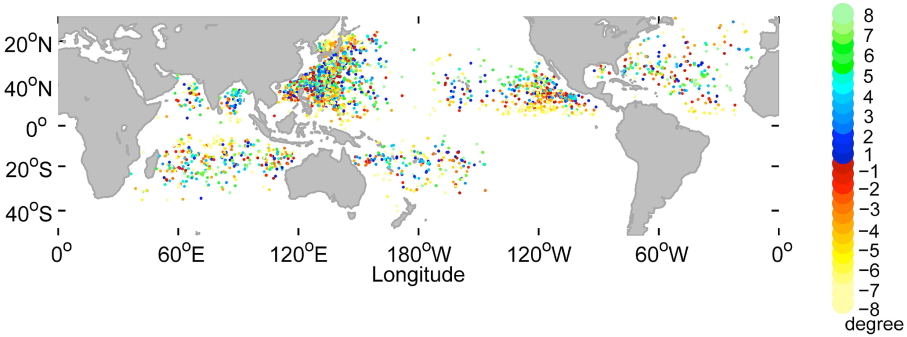

Figure 2. Locations of TC-affected Argo pairs with colors showing the cross-track distances of their locations relative to the corresponding storm track. Positive values indicate pairs to the right (left) side of the track in Northern Hemisphere (Southern Hemisphere).

OSD
11, 2831–2878, 2014

Global representation of tropical cyclone-induced ocean thermal changes

L. Cheng et al.

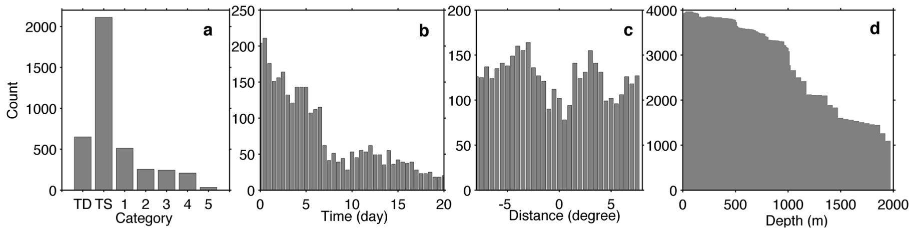

Figure 3. Histograms of the Argo float pairs for different statistics: **(a)** storm category, **(b)** time after storm passage (0.5 day bin), **(c)** distance from the storm center (0.5° bin), and **(d)** depth (10 m bin). In **(c)**, positive distance represents the right (left) side of the track in Northern Hemisphere (Southern Hemisphere), and negative distance represents the left (right) side in Southern Hemisphere (Northern Hemisphere).

OSD
11, 2831–2878, 2014

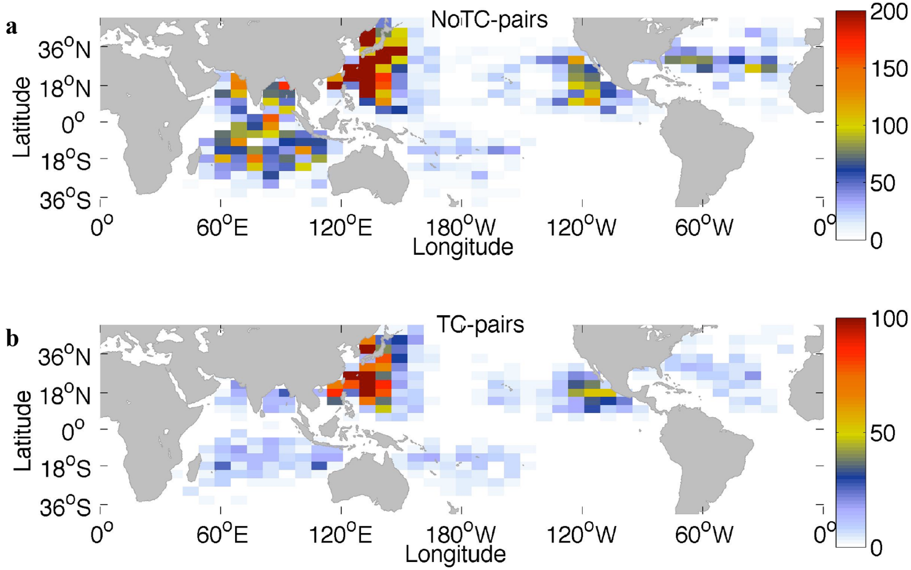

Figure 4. Counts of the **(a)** NoTC-pairs and **(b)** TC-affected pairs in each 4° by 8° degree grid box.

OSD
11, 2831–2878, 2014

Global representation of tropical cyclone-induced ocean thermal changes

L. Cheng et al.

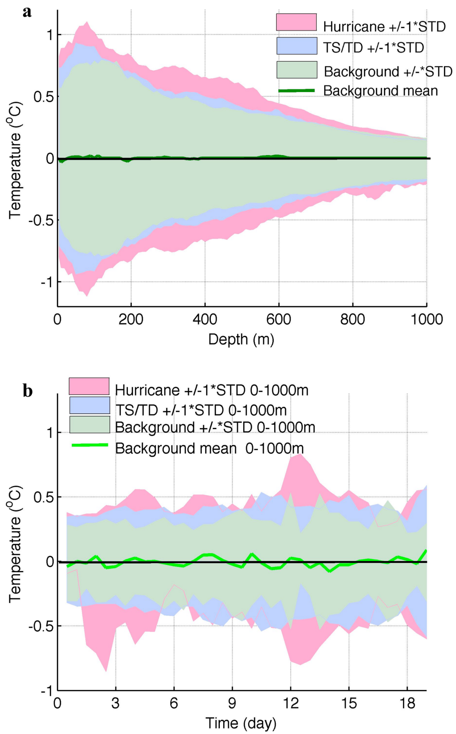

Figure 5. Background ocean temperature variability as a function of depth and time. **(a)** Mean (green curve) and one standard deviation (green shading) of background variability as a function of depth, compared with one standard deviation of hurricane and TS/TD affected pairs. **(b)** Time evolution of background variability of 0–1000 m average (light green line and light green shading for mean and standard deviation respectively). The standard deviations of temperature anomalies in Argo pairs under TS/TD and hurricane conditions are plotted in light blue and light red, respectively.

OSD
11, 2831–2878, 2014

L. Cheng et al.

Title Page
Abstract | Introduction
Conclusions | References
Tables | Figures
◂◂ | ▸▸
◂ | ▸
Back | Close
Full Screen / Esc
Printer-friendly Version
Interactive Discussion

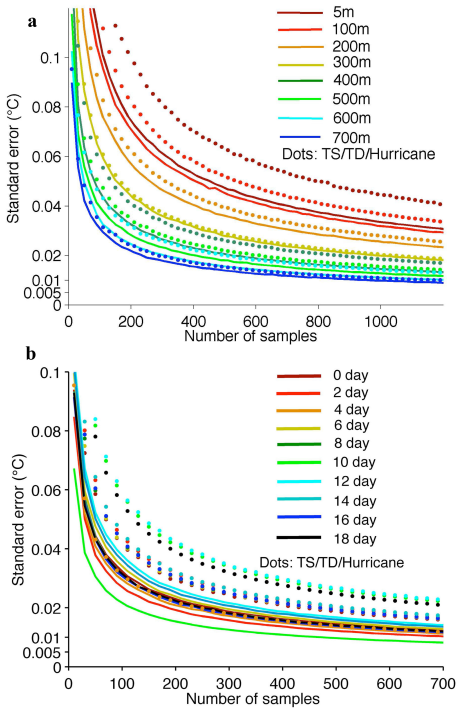

Figure 6. Bootstrap analyses of background noise. **(a)** Standard errors at different depth vs. sample numbers with colors denoting different depths. **(b)** Standard errors at different times vs. sample numbers with colors denoting different time. Solid lines are the results by using the whole NoTC-pairs dataset, and the dots show the same results for the TC-affected pairs.

OSD
11, 2831–2878, 2014

Global representation of tropical cyclone-induced ocean thermal changes

L. Cheng et al.

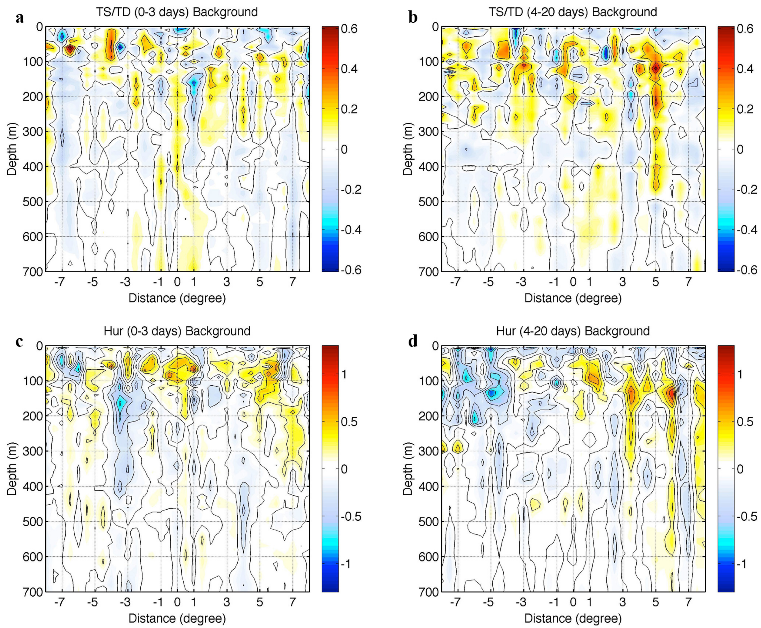

Figure 7. Background ocean thermal changes as a function of depth and distance in TC track coordinates. The background footprint is created corresponding to TS/TD footprint **(a)** on 0–3 days average and **(b)** on 4–20 days average, and to Hurricane footprint **(c)** on 0–3 days average and **(d)** on 4–20 days average. The contours interval is 0.2 °C in black. The units are °C.

OSD
11, 2831–2878, 2014

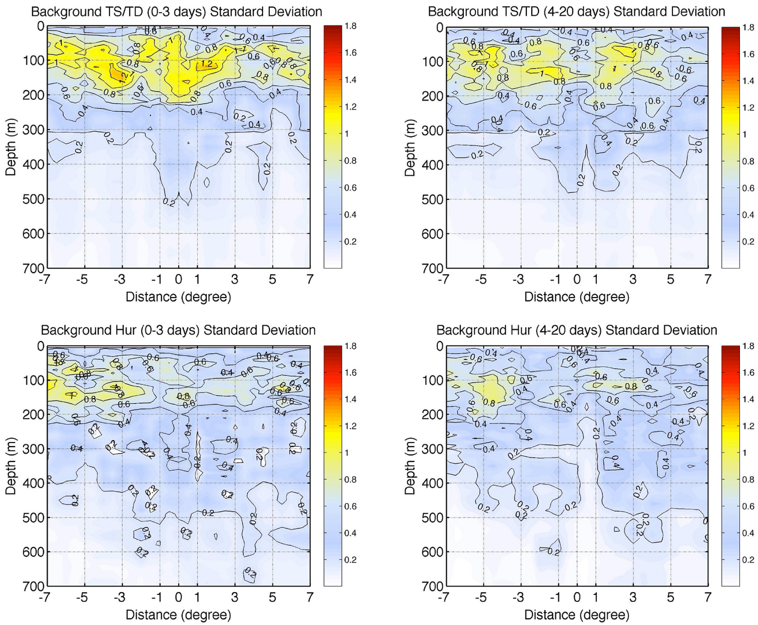

Figure 8. Standard deviation of the background footprints for TS/TD and Hurricane locations respectively on two time periods: 0–3 days and 4–20 days. The unit is °C.

OSD
11, 2831–2878, 2014

Global representation of tropical cyclone-induced ocean thermal changes

L. Cheng et al.

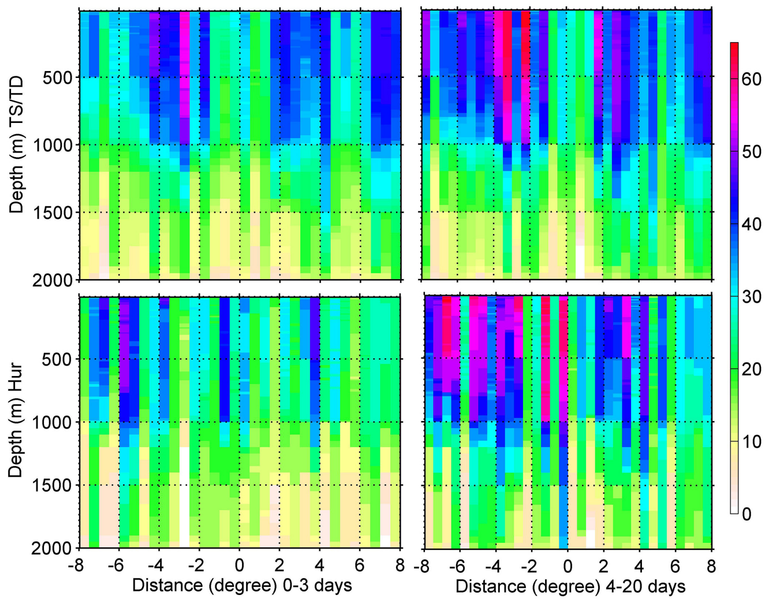

Figure 9. Count of TC-affected pairs in each 0.5° distance bin from −8° to 8° across the storm track for two footprint composites: TS/TD in the upper panel, Hurricane in the bottom panel. The statistics are conducted in two time periods: 0–3 days on the left, 4–20 days on the right.

OSD
11, 2831–2878, 2014

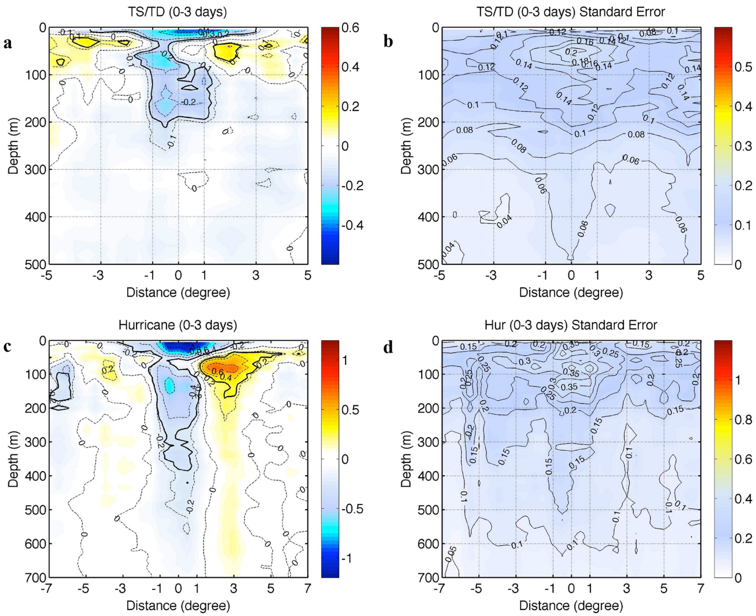

Figure 10. 0–3 days averaged thermal changes (relative to pre-storm conditions) as a function of depth and distance, in TC track coordinates. **(a)** TS/TD, between ±5° from track center, the dashed contours interval is 0.1 °C, and the solid black contours isolate the 90 % confidence interval of the signals. The standard error of the footprint is presented in **(b)**. **(c)** is 0–3 days footprint for Hurricane, between ±7° from track center, the dashed contours interval is 0.2 °C, and the solid black contours isolate the 90 % confidence interval of the signals. The standard error of the footprint is presented in **(d)**. The unit is °C.

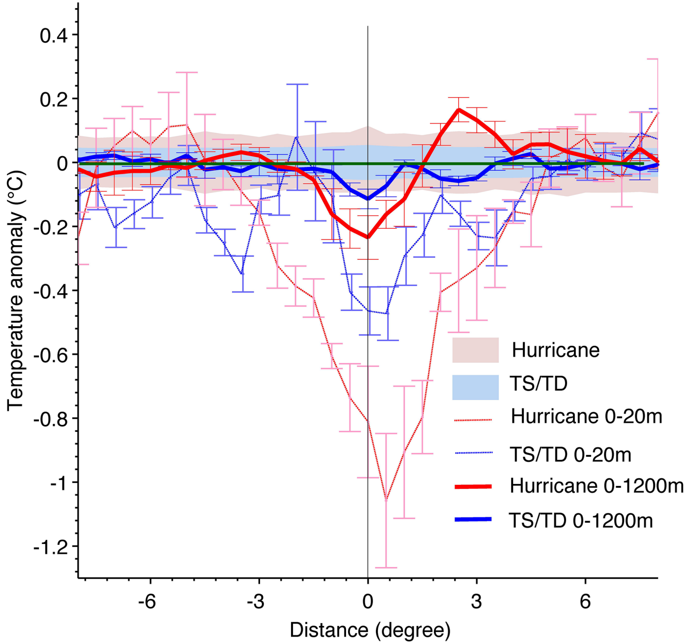

Figure 11. 0–3 days averaged temperature change as function of distance across the cyclone center for hurricanes (red) and TS/TD (blue), in TC track coordinates. The values are smoothed using a 3 point (1.5°) moving filter. Light blue shading shows the 90 % confidence interval of background noise based on Null-hypothesis analyses for TS/TD, and the light pink shading is for hurricane. Surface temperature anomalies are presented as the thin curves, and thick curves show 0–1200 m averaged temperature changes. The error bars are one standard deviation, which is calculated as follows: 90 % percent of pairs are randomly selected, and then we calculate the thermal anomalies of these pairs. This process is repeated 200 times, so 200 samples of thermal anomalies are obtained, and the standard deviation is calculated from thermal anomalies of these 200 samples.

OSD
11, 2831–2878, 2014

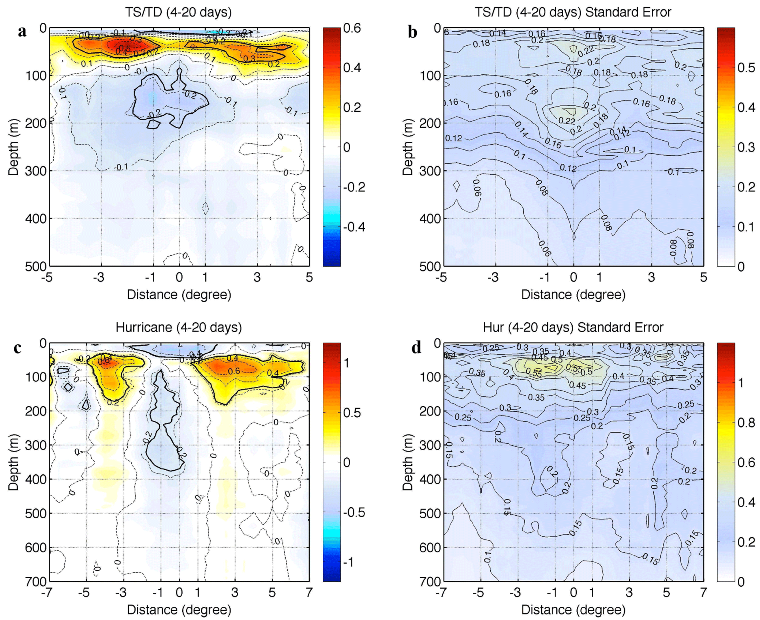

Figure 12. Vertical profile of the 4–20 days averaged ocean thermal changes (referenced to pre-storm conditions) from the track center for: **(a)** TS/TD between +5 and −5° and **(c)** Hurricanes between +7 and −7°. The dashed contours interval in black is 0.1 °C for TS/TD and 0.2 °C for Hurricane. The solid black contours denote the signals that are significant at 90 % confidence interval. **(b)** and **(d)** shows the standard error of the estimations corresponding to **(a)** and **(c)** respectively. The unit is °C.

OSD
11, 2831–2878, 2014

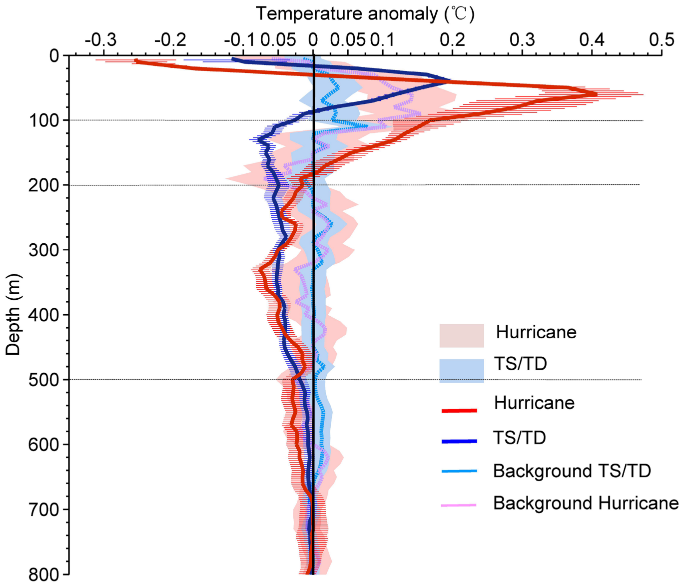

Figure 13. Vertical temperature change averaged within the −6 to +6° range from storm center during the recovery stage (4–20 days) relative to pre-storm conditions. Blue and red lines represent TS/TD and Hurricanes, respectively. Also plotted are the 90 % confidence intervals in Null-hypothesis test (light blue and light pink shading for TS/TD and hurricane, respectively). The light blue and pink curves show the mean background noise in TS/TD and Hurricane subsets respectively. The error bars represent the standard deviations, which are calculated by using the method as presented in Fig. 11.

OSD
11, 2831–2878, 2014

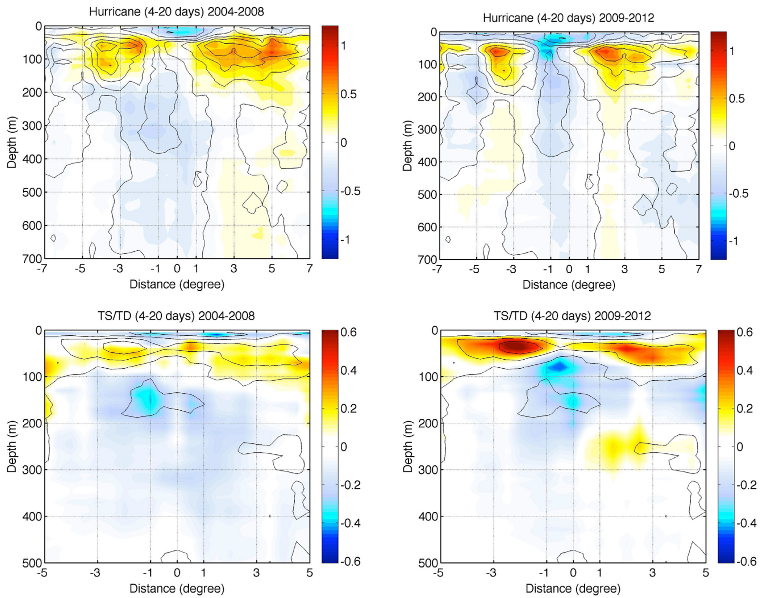

Figure 14. The 4–20 days averaged ocean thermal changes detected by using data from two year periods: 2004–2008 in the left panel and 2009–2012 in the right panel, shown in colors. The black contours are the result when using all of the data from 2004 to 2012, the same to the contours in Fig. 12. The results of Hurricane are presented in the top panel and the bottom panel for TS/TD. The unit is °C.

OSD
11, 2831–2878, 2014

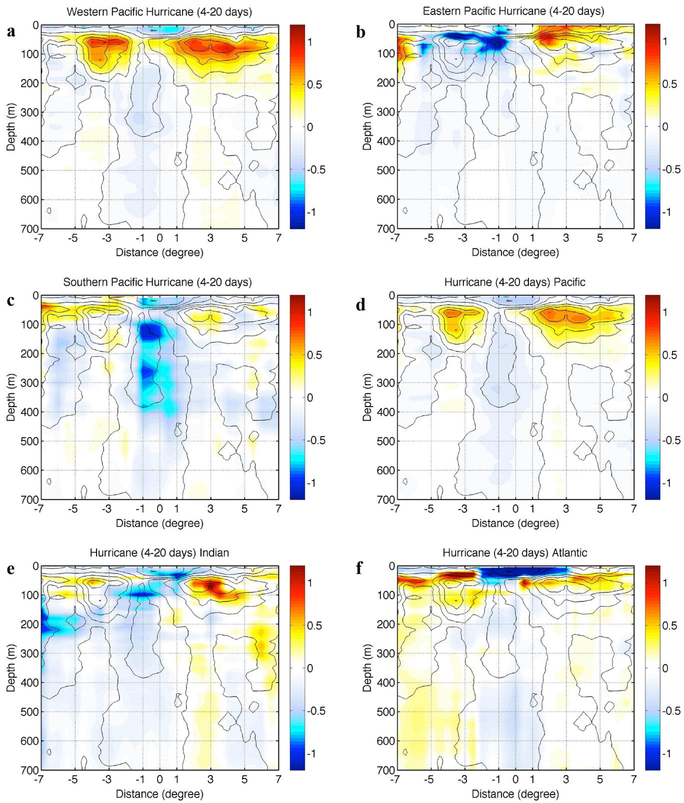

Figure 15. Ocean thermal changes induced by hurricanes within 4–20 days after storm passage for individual ocean basins: **(a)** in Western Pacific Ocean, **(b)** in Eastern Pacific Ocean, **(c)** in Southern Pacific Ocean, **(d)** in Pacific Ocean, **(e)** in Indian Ocean, **(f)** in Atlantic Ocean. The black contour is the global-averaged hurricane-induced ocean thermal changes in 4–20 days, which is the same to that in Fig. 12c. The unit is °C.

OSD
11, 2831–2878, 2014

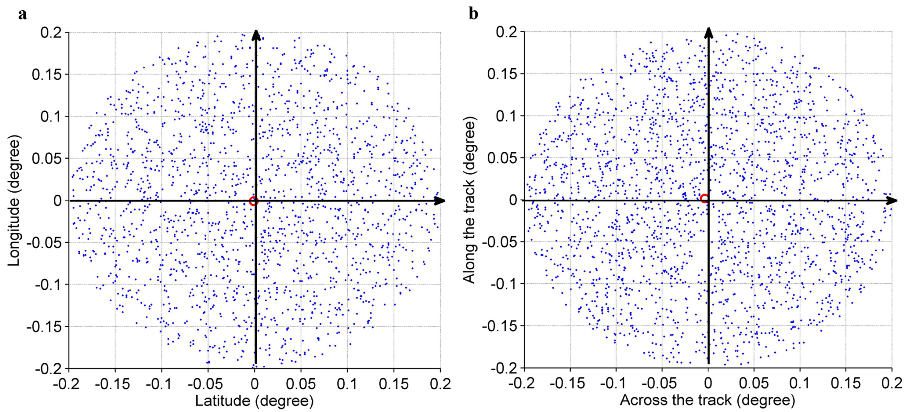

Figure A1. Schematic scatter plots showing Argo floats drifting destination from the origin. Two coordinate systems are: **(a)** latitude–longitude, with the location of the float before storm as origin; **(b)** Track direction as *y* axis, and the location of the float before the storm as the origin. The red dots are the destination of the pairs with pairs from the same float in red (with the mean in red star) pairs from different floats in blue (with the mean in big blue dot).

OSD
11, 2831–2878, 2014

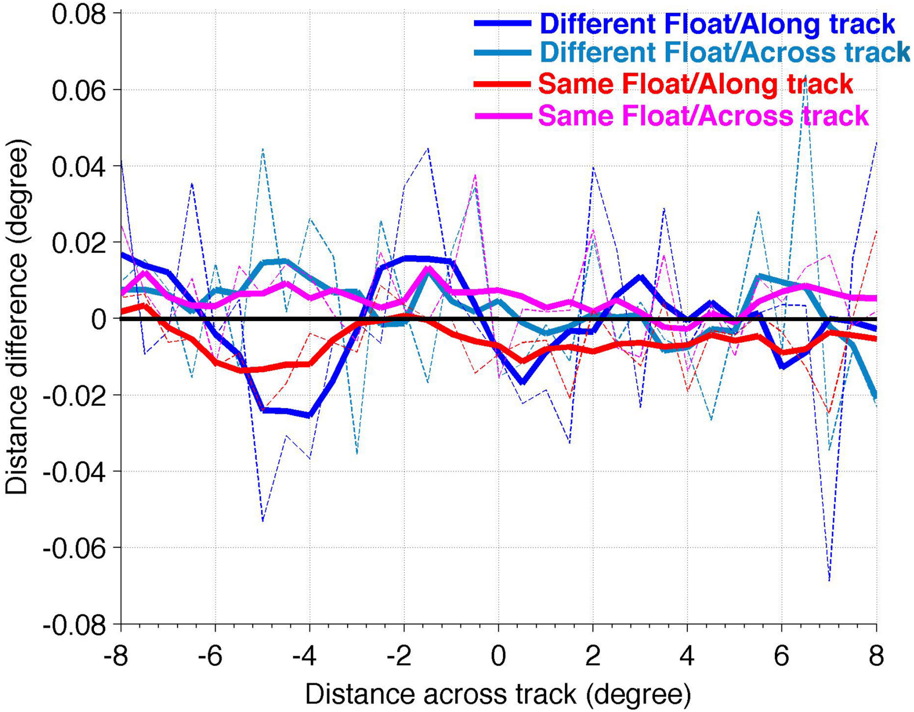

Figure A2. Horizontal distance difference between the two profiles in a TC-affected pair along and across the track as a function of the distance from the float location to the track center. Here the distance is calculated in track coordinates, i.e: positive distance across the track represents the inertial-resonant side (right side in Northern Hemisphere and left side in Southern Hemisphere). The horizontal distances by using pairs that the two profiles are from different floats are shown in dark blue (along track) and light blue (across track), while drifting distances based on the remaining pairs are shown in purple (across track) and red (along track).

OSD
11, 2831–2878, 2014